Journal of Materials Chemistry C

PAPER

View Article Online
View Journal | View Issue

Cite this: J. Mater. Chem. C, 2018, 6, 4095

High-performance red electrophosphorescent devices based on all-solution-processed hydrogen-bonded supramolecular material†

Cheng Zhang, ‡*[a] Hui Zeng,‡[a] Qingyu Huang,‡[b] Yi Wang,[a] Yongshuai Chai,[c] Yan Huang, [a] Suling Zhao *[b] and Zhiyun Lu *[a]

An oligoamide strand bearing a guest phosphorescent unit, named **4HB-Irpiq**, was designed and synthesized. The guest hydrogen-bonded strand **4HB-Irpiq** could self-assemble *via* hydrogen-bonding interactions with the host hydrogen-bonded strand **4HB-CzNI** into a hydrogen-bonded supramolecule, named **4HB-Irpiq-CzNI**. In comparison with physical blends of the guest counterpart **Irpiq** with host small molecule **CzNI**, **4HB-Irpiq-CzNI** shows a more efficient energy transfer process between host and guest in both dilute solution and doped film state, which could be attributed to the shortened spatial distance between the host and guest units. Moreover, compared with **Irpiq**, **4HB-Irpiq-CzNI** shows a higher photoluminescence quantum yield in the neat-film state, indicating that **4HB-Irpiq-CzNI** could be better at alleviating concentration quenching. As a consequence, a phosphorescent organic light-emitting diode with **4HB-Irpiq-CzNI** and **Irpiq** as the light-emitting dopant has been fabricated based on all-solution-processing. The results indicate that OLEDs with **4HB-Irpiq-CzNI** show dramatically improved performance over the counterpart **Irpiq**: with a lower turn-on voltage (6.0 *vs.* 7.6 V), higher maximum luminance (6446 *vs.* 2543 cd m^{-2}) and current efficiency (7.0 *vs.* 4.3 cd A^{-1}) as well as a lower efficiency roll-off. The hydrogen-bonded supramolecular **4HB-Irpiq-CzNI** material shows one of the best performances among all-solution-processed red PhOLEDs.

Received 15th December 2017,
Accepted 13th March 2018

DOI: 10.1039/c7tc05764d

rsc.li/materials-c

1. Introduction

Phosphorescent organic light-emitting diodes (PhOLEDs) have been recognized as one of the most promising candidates for full-color large-area flat-panel displays and solid-state lighting sources.[1–3] Since phosphorescent complexes can harvest both singlet and triplet excitons, which can potentially ensure nearly 100% internal quantum efficiency, they have been extensively developed as high-efficiency PhOLEDs.[4–8] In particular, cyclometalated iridium complexes with short lifetimes in the excited state and high luminescence efficiencies have attracted enormous research attention.[9–16] Recently, solution-processable electroluminescent (EL) materials have attracted extensive attention due to their low-cost and large-area OLED displays and lighting.[17–21] In this context, electrophosphorescent polymers or dendritic molecules are of particular interest for their ready solution processability, which allows the utilization of less expensive spin-coating and ink-jet printing methods for the preparation of large-area devices.[22–24] However, some challenges still exist in developing high-performance solution-processed PhOLEDs. For instance, polymers generally suffer from batch-to-batch variations in molecular structure and low purity, and dendritic molecules suffer from shortcomings in their purification procedures and have quite elaborate and tedious synthesis.[25–27]

E. W. Meijer[28] *et al.* reported the pioneering work of using hydrogen-bonded supramolecular copolymers for OLEDs. This opens up a new way to obtain high-performance EL materials. The hydrogen-bonded supramolecular materials exhibit many advantages, such as good filmic properties, high purity without batch-to-batch variation, well-defined molecular structures, and facile synthesis as well. Recently, our group has reported a hydrogen-bonded self-assembly supramolecular electroluminescent material, which achieved relatively high performance. The maximum luminance and current efficiency are 5260 cd m^{-2} and 3.5 cd A^{-1} respectively.[29]

[a] Key Laboratory of Green Chemistry and Technology of Ministry of Education, College of Chemistry, Sichuan University, Chengdu, 610064, P. R. China. E-mail: zhangchengchem@sina.com, luzhiyun@scu.edu.cn
[b] Key Laboratory of Luminescence and Optical Information of Ministry of Education, Institute of Optoelectronics Technology, Beijing Jiaotong University, Beijing, 100044, P. R. China. E-mail: slzhao@bjtu.edu.cn
[c] Interdisciplinary Research Center on Biology and Chemistry, Shanghai Institute of Organic Chemistry, Chinese Academy of Sciences, Shanghai, 200032, P. R. China

† Electronic supplementary information (ESI) available. See DOI: 10.1039/c7tc05764d

‡ These authors contributed equally.

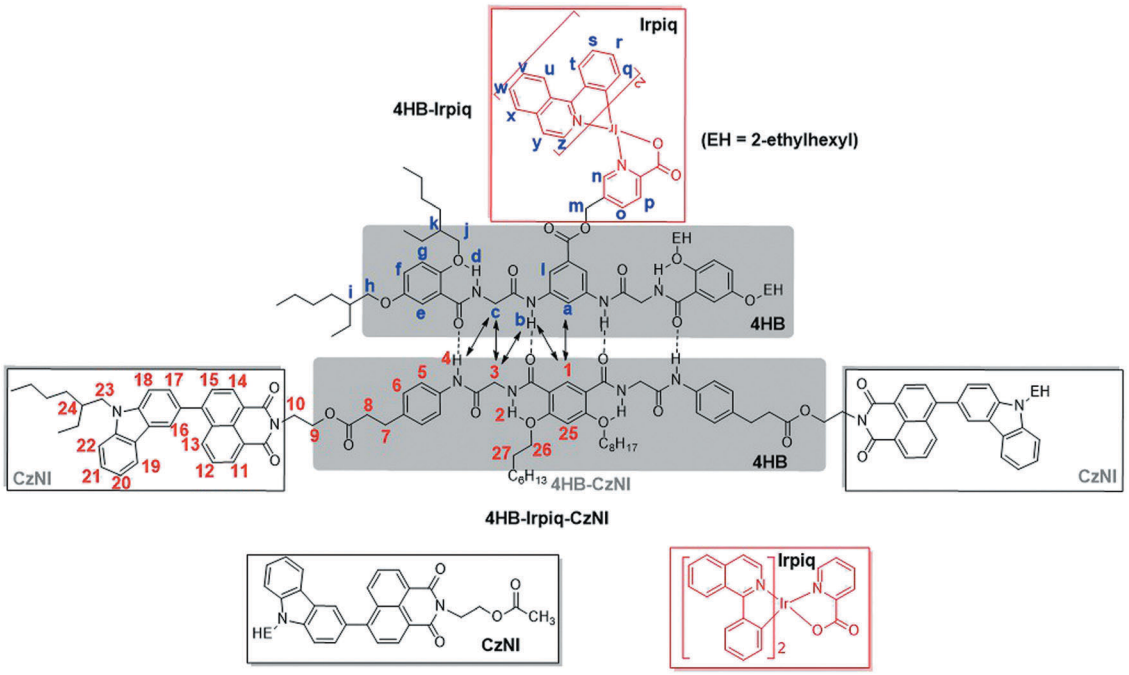

Fig. 1 Molecular structures of guest single strand **4hb-irpiq**, the host single strand **4hb-czni**, the hydrogen-bonding supramolecular **4hb-irpiq-czni**, and the small molecular reference compounds **czni** and **irpiq**. Here, eh denotes 2-ethylhexyl group.

In this contribution, we introduce a red phosphorescent small molecule **Irpiq** to an oligoamide strand with hydrogen-bonding sequence ADDA as a guest hydrogen-bonded strand which was named **4HB-Irpiq**. In order to find a host to form an efficient energy transfer pair with **Irpiq**, we chose the fluorescent small molecule **CzNI** as the host, because the absorption spectrum of **Irpiq** has an effective spectral overlap with the emission spectrum of **CzNI** (Fig. S1, ESI†), so they may constitute an efficient energy transfer pair.[30,31] And we connect the **CzNI** into a complementary hydrogen-bonding sequence DAAD with **4HB-Irpiq** to form **4HB-CzNI** as the host hydrogen-bonded strand, as has been reported recently.[29] The molecular structures of the host single strand **4HB-CzNI**, guest single strand **4HB-Irpiq**, the objective hydrogen-bonded supramolecular **4HB-Irpiq-CzNI** as well as the small molecular host and guest reference compounds **CzNI** and **Irpiq** are shown in Fig. 1.

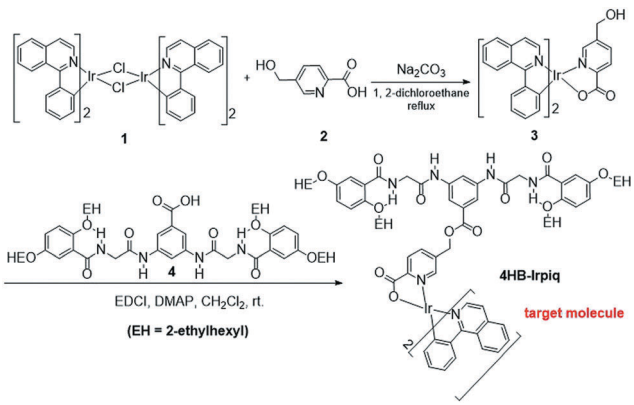

Scheme 1 Synthetic route to the target compound **4hb-irpiq**.

2. Results and discussion

2.1. Synthesis and structural characterization

Target molecule **4HB-Irpiq** was synthesized (Scheme 1). The small molecules of the host and guest luminogens and **4HB-CzNI** were synthesized according to reports in the literature.[29–32] The molecular structure of the target compound was confirmed by ^{1}H NMR, ^{13}C NMR and high-resolution MS.

^{1}H NMR studies of hydrogen-bonded single strands of **4HB-CzNI** and **4HB-Irpiq** in 30 mM $CDCl_3$ solution revealed: shifts in the aniline NH signals of **4** for **4HB-CzNI** located at 9.25 ppm and shifts in the aniline NH signals of **b** for **4HB-Irpiq** located at 8.96 ppm. Compared to the hydrogen-bonded single strands of **4HB-CzNI** and **4HB-Irpiq**, the mixture of these two hydrogen-bonded single strands (1 : 1 in molar ratio) in 30 mM $CDCl_3$ solution revealed downfield shifts of the aniline NH signals of **4** and **b** appearing at 10.03 ppm and 10.17 ppm, respectively, which suggests the formation of hydrogen-bonded supramolecular **4HB-Irpiq-CzNI** (Fig. 2). Furthermore, the disappearance of the aniline NH signals of **4** and **b** for single strands of **4HB-CzNI** and **4HB-Irpiq**, respectively, indicated that hydrogen-bonded single strands of neither **4HB-CzNI** nor **4HB-Irpiq** exited the uncomplexed strands. This provided direct evidence for the formation of hydrogen-bonded supramolecular **4HB-Irpiq-CzNI**.

Furthermore, to provide more detailed evidence for the formation of hydrogen-bonded supramolecular **4HB-Irpiq-CzNI** in solution, 2D ^{1}H NMR (NOESY) spectra were recorded on a Bruker-AVANCE-II-600 (Fig. 3). Hydrogen-bonded single strands

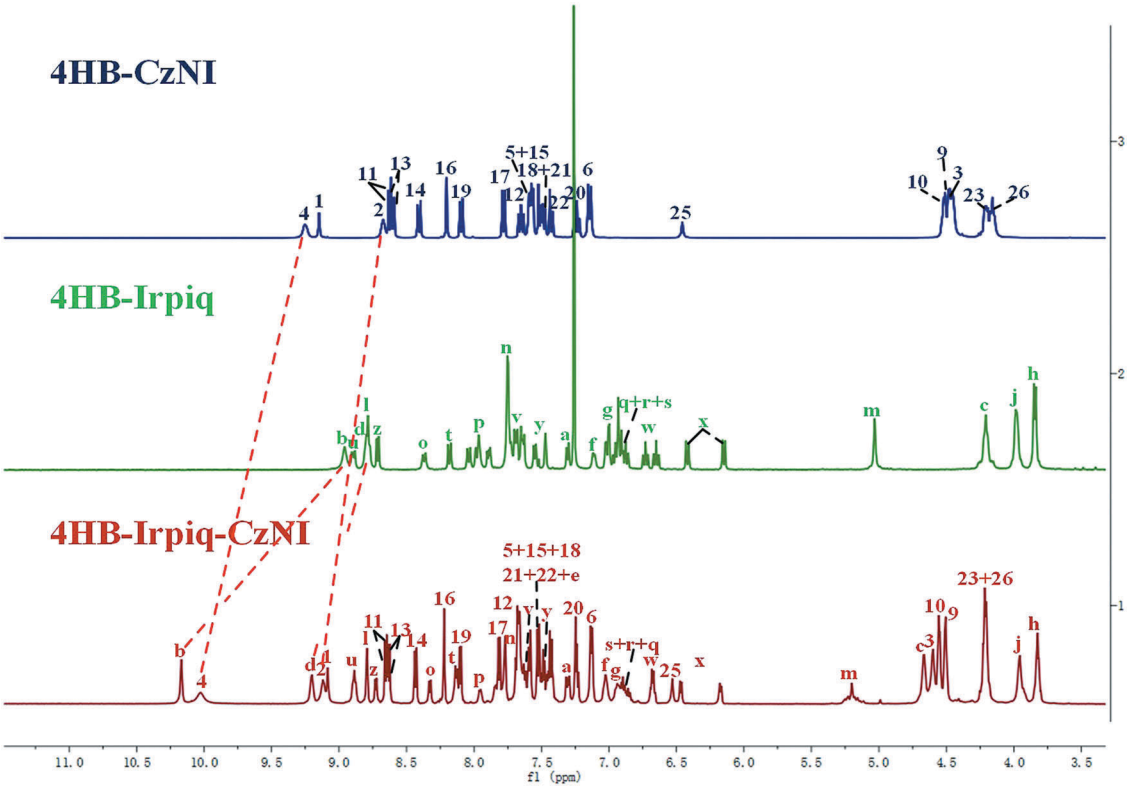

Fig. 2 Partial 1D ^{1}H NMR spectra of **4hb-czni**, **4hb-irpiq** and the 1 : 1 mixture of **4hb-czni** and **4hb-irpiq**. Spectra recorded in 30 mm $CDCl_3$ solutions.

of **4HB-CzNI** and **4HB-Irpiq** were mixed (1 : 1 in molar ratio) in 30 mM $CDCl_3$ solution. It is obvious that strong interstrand contacts exist, and there are strong NOE contacts between protons **1** and **a**, **1** and **b**, **3** and **b**, **3** and **c**, **4** and **c**, **5** and **e**, suggesting the successful self-assembly of **4HB-CzNI** and **4HB-Irpiq** into hydrogen-bonded supramolecular **4HB-Irpiq-CzNI**.[33–36]

2.2. Photophysical properties

The UV-vis absorption spectra of the hydrogen-bonded single strands of **4HB-CzNI**, **4HB-Irpiq** and the hydrogen-bonded supramolecular **4HB-Irpiq-CzNI** as well as the small molecular counterpart **Irpiq** in dilute solution (10^{-5} mol L^{-1} in CH_2Cl_2) and thin solid film states are shown in Fig. 4a and b, and the corresponding data are summarized in Table 1. In the region of 350–600 nm, the absorption spectrum of a dilute solution sample of **4HB-Irpiq** nearly resembles that for the counterpart **Irpiq**, while the absorption spectrum of a 1 : 1 mixture of **4HB-CzNI** and **4HB-Irpiq**, the hydrogen-bonded supramolecular **4HB-Irpiq-CzNI**, is just a simple superposition of those for hydrogen-bonded single strands of **4HB-CzNI** and **4HB-Irpiq**. In the thin solid film state, the target compound **4HB-Irpiq** and hydrogen-bonded supramolecular **4HB-Irpiq-CzNI** show slightly red-shifted and broadened absorption spectra compared to their corresponding solution samples (Fig. 4b), while the small molecular compound **Irpiq** shows a relatively heavy red-shift compared to that of **4HB-Irpiq** and **4HB-Irpiq-CzNI**. Moreover, according to tapping-mode AFM height images (Fig. 5), the morphologies of **Irpiq** and **4HB-Irpiq** are drastically different in the thin solid film state. This indicates that the molecular packing of the small molecular compound **Irpiq** should be more intensive than that of **4HB-Irpiq** in the thin film state. Therefore, the incorporation of the hydrogen-bonded self-assembled oligoamide strand into the guest **Irpiq** would be beneficial to the alleviation of molecular packing of the luminogens, leading to suppressed concentration quenching, which is consistent with the experimental findings we reported previously.[37,38]

The photoluminescence (PL) spectra of the small molecular compound **Irpiq** and target compound **4HB-Irpiq** and hydrogen-bonded supramolecular **4HB-Irpiq-CzNI** in dilute solution (10^{-5} mol L^{-1} in CH_2Cl_2) and thin solid film state are illustrated in Fig. 4c and d. In dilute solution, the PL emission band of **4HB-Irpiq** (λ_{PL} = 606 nm) is also the superposition of **Irpiq** (λ_{PL} = 606 nm) (Fig. 4c and Table 1). While in the thin solid film state, the PL emission band of **Irpiq** (λ_{PL} = 624 nm) has a red-shifted emission spectrum compared to that of **4HB-Irpiq** (λ_{PL} = 612 nm) (Fig. 4d), confirming that the introduction of the hydrogen-bonded strand moiety into the small molecular compound **Irpiq** luminogen could benefit the alleviation of π–π stacking of the **Irpiq** unit, which would result in suppressed concentration quenching of the guest unit in the condensed state. This deduction was further confirmed by the PL quantum yield (PLQY) characterization results, in the thin film state: the absolute PLQY of **Irpiq** film is 0.00, but that of the **4HB-Irpiq** sample is 0.16, suggesting that the oligoamide strand bearing the guest **Irpiq** is propitious to the suppression of the stacking of chromophores.

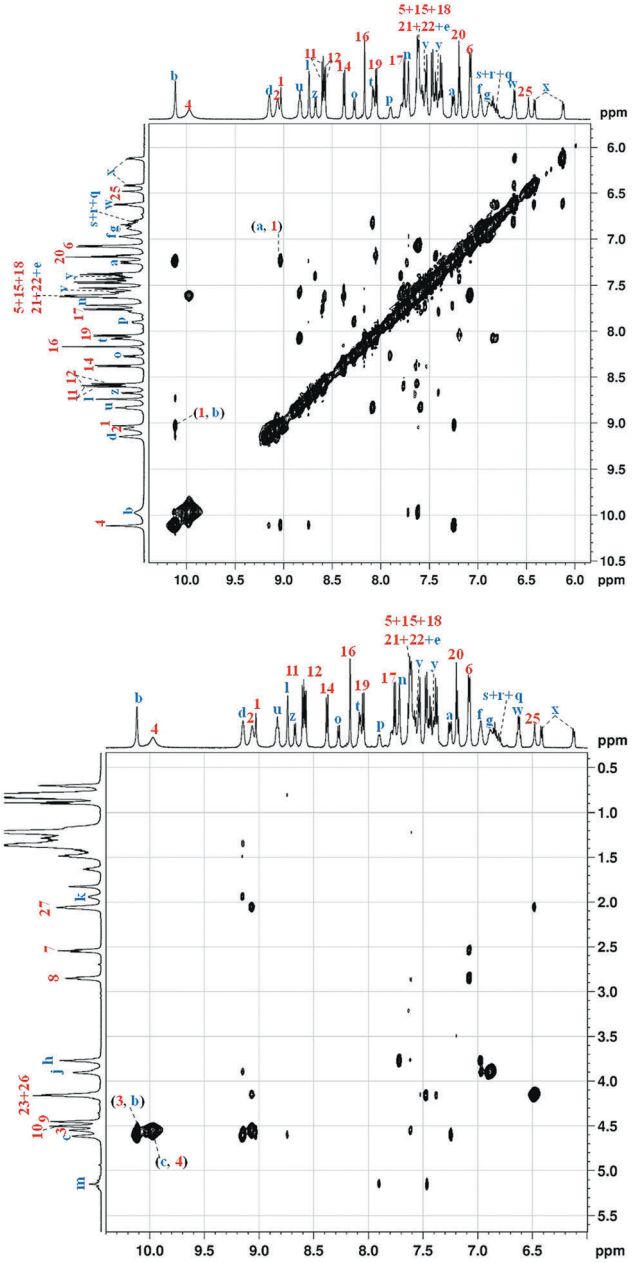

Fig. 3 2D ^{1}H NMR spectra (NOESY) spectra of the 1 : 1 mixture of **4hb-czni** and **4hb-irpiq**. Spectra recorded in 30 mm $CDCl_3$ solutions.

In dilute solution, the hydrogen-bonded supramolecular **4HB-Irpiq-CzNI** sample exhibits dual fluorescence (λ_{PL} = 550 nm, 606 nm) comprising the emission bands of both host (**4HB-CzNI**) and guest (**4HB-Irpiq**) (Fig. 4c); while in the thin solid film state, it exhibits just one emission band (λ_{PL} = 613 nm), which should be attributed to the emission from the guest **Irpiq** moiety (Fig. 4d). As a consequence, more efficient energy transfer between host **CzNI** and guest **Irpiq** luminogens should exist in the thin solid film than in dilute solution in the **4HB-Irpiq-CzNI** moiety, which should be attributed to the closer distances between the host and guest in the condensed state. Furthermore, the neat-film sample of **4HB-Irpiq-CzNI** shows a relatively higher φ_{PL} of 0.19 than that of the small molecular counterpart **Irpiq** (φ_{PL} = 0.00) and target molecular **4HB-Irpiq** (φ_{PL} = 0.16). This suggests that: (1) compared with the small molecular counterpart **Irpiq** in thin-film, the **4HB-Irpiq-CzNI** could suppress the concentration quenching of the guest unit; (2) compared with the target molecular **4HB-Irpiq** in thin-film, there was effective energy transfer in **4HB-Irpiq-CzNI**.

As shown in Fig. 6a, the steady-state fluorescence spectrum of the hydrogen-bonded supramolecular **4HB-Irpiq-CzNI** component showed a weaker band than that of single strand **4HB-CzNI** (quenched 60%, emission monitored at band **I**). At the same time, compared with band **II** which belongs to **4HB-Irpiq**, the fluorescence intensity of the hydrogen-bonded supramolecular **4HB-Irpiq-CzNI** is increased. This clearly suggests that energy transfer has occurred from **4HB-CzNI** to **4HB-Irpiq**.[39,40] In **4HB-Irpiq-CzNI** the energy transfer is further investigated by using the fluorescence excitation spectrum. Fig. 6b shows the excitation spectrum of **4HB-Irpiq-CzNI** collected at 690 nm where only the **4HB-Irpiq** emission exists. The overlap of the excitation spectra with the corresponding absorption spectra with respect to **4HB-Irpiq-CzNI** revealed that the energy transfer efficiency is ~60%.[39,40] The calculation method for energy transfer efficiency is the area ratio of corrected excitation spectra with the normalized corresponding absorption spectra for **4HB-Irpiq-CzNI**. Therefore, it is suggested that the fluorescence of the host **4HB-CzNI** is quenched by the guest **4HB-Irpiq** due to the energy transfer process.

The time-resolved PL measurements could further prove that the energy transfer process occurred in **4HB-Irpiq-CzNI**. As shown in Fig. 6c, initially we observed energy transfer processes in **4HB-Irpiq-CzNI**, which came from the host single strand **4HB-CzNI** in the absence or presence of the guest **4HB-Irpiq** compound in dilute solution (λ_{ex} = 368 nm). The average lifetime of the host fluorophore **4HB-CzNI** was determined to be 3.66 ns; and the average lifetime of the host **4HB-CzNI** fluorophore decreased heavily to 0.95 ns with the addition of 1.0 equiv. of guest **4HB-Irpiq**. The energy transfer efficiency could also be measured using the relative lifetimes of the host, in the absence (τ_D) and presence (τ_{DA}) of the guest by using eqn (1):

$$E = 1 - \tau_{DA}/\tau_D \quad (1)$$

However, the result of the calculation showed that the energy transfer efficiency was ~74%, which was more than ~60%. This suggests that there existed an intermolecular energy transfer of ~14% because of some of unsuccessful hydrogen-bonded self-assembly between the host **4HB-CzNI** and the guest **4HB-Irpiq** in dilute solution.

Furthermore, when fluorescence decay traces (λ_{ex} = 368 nm) were monitored at 690 nm, we observed that the lifetime of the guest **4HB-Irpiq** was determined to be 1.11 μs; and the lifetime of the **4HB-Irpiq-CzNI** increased to 1.69 μs (Fig. 6d). This suggested an energy transfer process between **4HB-CzNI** and **4HB-Irpiq** moieties in **4HB-Irpiq-CzNI**.[41]

In order to investigate whether the hydrogen-bonded supramolecular **4HB-Irpiq-CzNI** could display more efficient energy

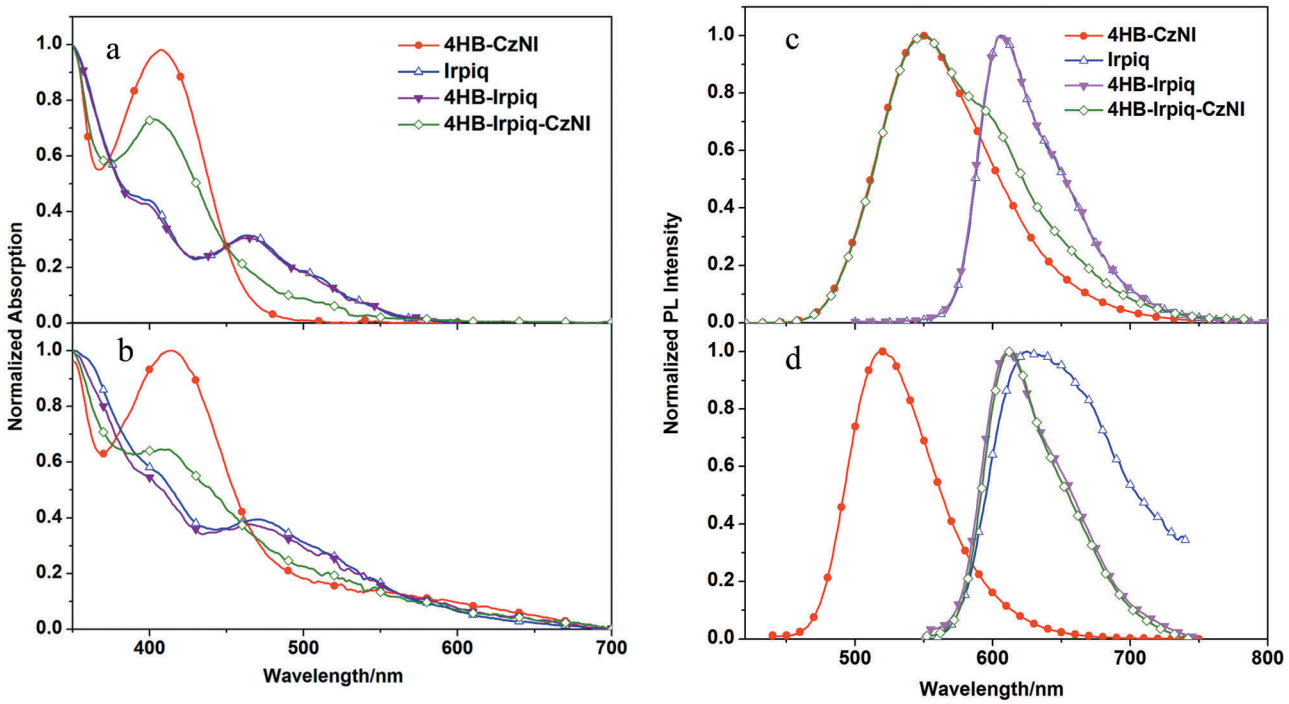

Fig. 4 UV-Vis absorption spectra of **4hb-czni**, **irpiq**, **4hb-irpiq** and **4hb-irpiq-czni** in: (a) dilute CH_2Cl_2 solution; and (b) thin-film state. PL emission spectra of **4hb-czni**, **irpiq**, **4hb-irpiq** and **4hb-irpiq-czni**. (c) In dilute CH_2Cl_2 solution; (d) in thin film state.

Table 1 Photophysical, electrochemical and thermal stability data of **Irpiq**, **4HB-Irpiq** and **4HB-Irpiq-CzNI**

Compound	$\lambda_{abs}{}^a$ (nm)	$\lambda_{abs}{}^b$ (nm)	$\lambda_{PL}{}^a$ (nm)	$\lambda_{PL}{}^b$ (nm)	$\varphi_{PL}{}^c$	$E^{ox}_{ons}{}^d$ (V)	HOMO^e (eV)	$E^g_{opt}{}^f$ (eV)	LUMO^g (eV)	T_d (°C)
Irpiq	398, 465	399, 471	606	624	0.00	0.54	−5.34	2.22	−3.12	—
4HB-Irpiq	397, 465	399, 462	606	612	0.16	0.55	−5.35	2.23	−3.12	254
4HB-Irpiq-CzNI	403	412	550, 606	613	0.19	0.52	−5.32	2.59	−2.73	320

[a] Measured in 10^{-5} mol L^{-1} CH_2Cl_2 solution. [b] Measured in neat-film state. [c] Absolute PL quantum yields of the neat-film samples determined using an integrating sphere at 298 K. [d] Oxidation potential values measured in CH_2Cl_2 solutions containing 5×10^{-4} mol L^{-1} of the compounds, referred internally to Fc/Fc^+. [e] HOMO energy levels deduced from the equation of HOMO = $-(4.8 + E^{ox}_{ons})$. [f] Optical bandgaps estimated from the onset wavelength of the optical absorption bands. [g] LUMO energy levels obtained from the equation of LUMO = HOMO + E^g_{opt}.

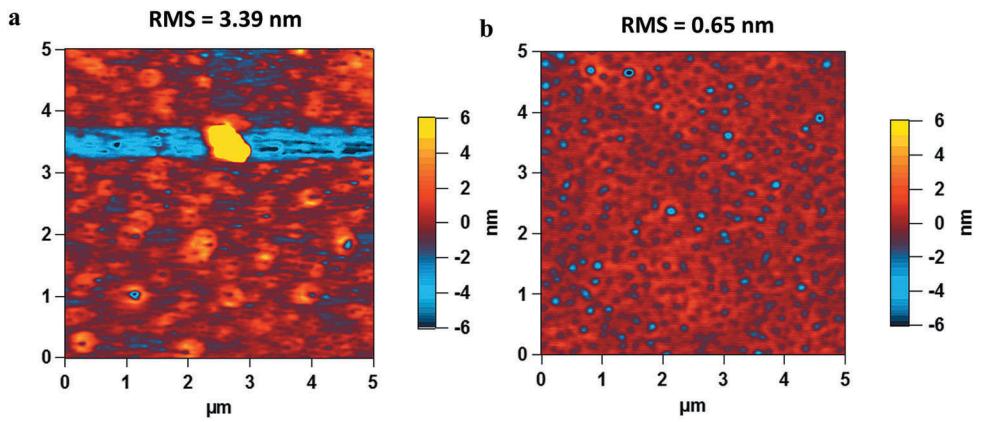

Fig. 5 Tapping-mode AFM height images (5 × 5 μm) of (a) **irpiq** and (b) **4hb-irpiq** films.

transfer processes in the condensed state, we fabricated two doped neat-films of same concentration with identical host (**CzNI**: 1.64 mol kg^{-1}) and guest (**Irpiq** and **4HB-Irpiq-CzNI**: 0.11 mol kg^{-1}) molalities. As shown in Fig. 6e, for the **Irpiq**-doped and **4HB-Irpiq-CzNI**-doped film samples, the PL emission band of the host fluorophore could be observed; and in the **Irpiq**-based

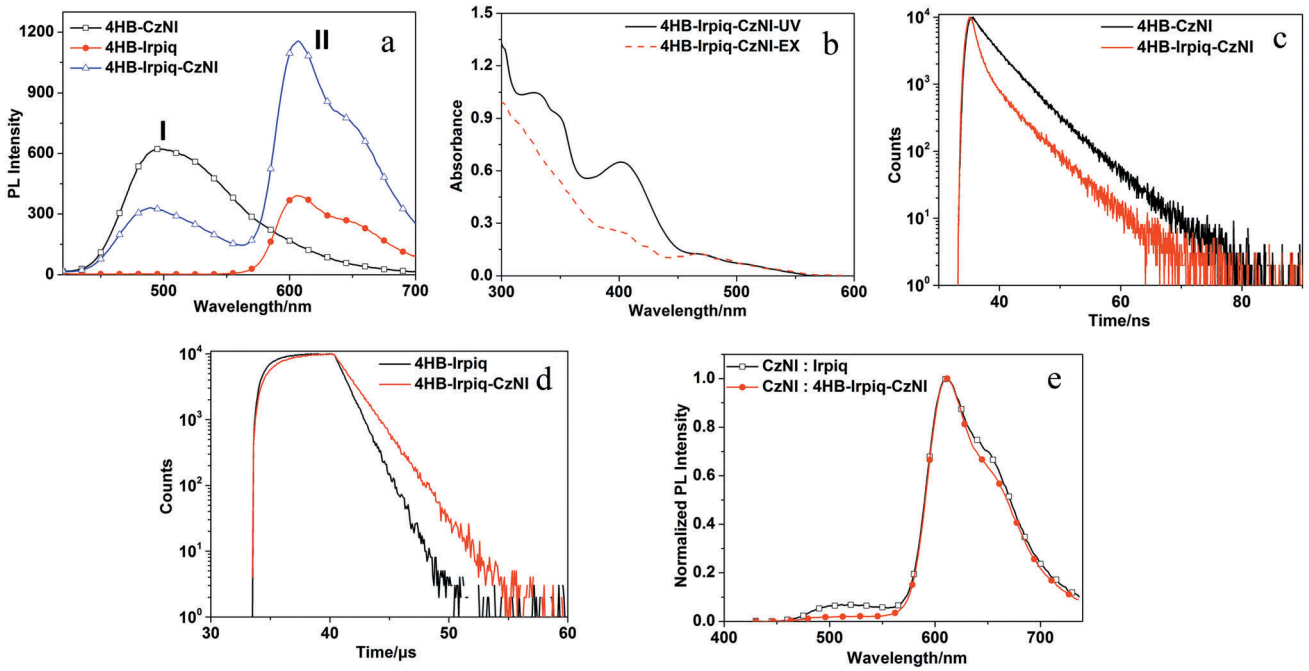

Fig. 6 (a) Steady-state fluorescence spectra of **4hb-czni**, **4hb-irpiq** and **4hb-irpiq-czni** with excitation at 368 nm in 10^{-6} mol L^{-1} toluene : dichloromethane = 9 : 1 solution. (b) Absorption (solid) and corrected fluorescence excitation (dashed) spectra of the **4hb-irpiq-czni** in 10^{-6} mol L^{-1} toluene : dichloromethane = 9 : 1 solution, and the spectra were normalized between 470 and 550 nm. The excitation spectrum was collected at 690 nm corresponding to the emission of **4hb-irpiq**. (c) Fluorescence decay curves of **4hb-czni** and **4hb-irpiq-czni**. (Recorded in 10^{-6} mol L^{-1} toluene : dichloromethane = 9 : 1 solution, λ_{ex} = 368 nm, λ_{em} = 490 nm). (d) Fluorescence decay curves of **4hb-irpiq** and **4hb-irpiq-czni**. (Recorded in 10^{-6} mol L^{-1} toluene : dichloromethane = 9 : 1 solution, λ_{ex} = 368 nm, λ_{em} = 690 nm.) (e) PL emission spectra of the doped film samples with **czni** (molality: 1.64 mol kg^{-1}) as the host component, **irpiq** and **4hb-irpiq-czni** as the guest component (molality: 0.11 mol kg^{-1}) (λ_{ex} = 368 nm).

film sample, the emission intensity of the fluorescence of the host is higher (λ_{ex} = 368 nm). While negligible host emission is discernable in the **4HB-Irpiq-CzNI**-doped film. Taking into consideration that the molar compositions of the host and guest chromophores are identical in these two neat-films, more efficient energy transfer processes should exist in the **4HB-Irpiq-CzNI**-based film.

2.3. Electrochemical, computational and thermal studies

The electrochemical behaviours of **Irpiq**, **4HB-Irpiq** and **4HB-Irpiq-CzNI** were probed by cyclic voltammetry in degassed dichloromethane solution. As shown in Fig. 7 and Table 1, the oxidation potentials of **Irpiq** and **4HB-Irpiq** are 0.54 V and 0.55 V, respectively. Hence their HOMO energy levels were estimated to be −5.34 eV and −5.35 eV according to the equation HOMO = $-(4.8 + E_{ox}^{ons})$, and their LUMO energy levels were estimated to be −3.12 eV and −3.12 eV according to the equation LUMO = HOMO + E_g. Therefore, the HOMO and LUMO energy levels of **Irpiq** and **4HB-Irpiq** are rather similar. This illustrates that the quadruple H-bond oligoamide unit (**4HB**) would have almost no influence on the frontier molecular orbital energy levels of **Irpiq**. However, the oxidation potential of **4HB-Irpiq-CzNI** is 0.52 V, the HOMO energy level is estimated to be −5.32 eV, and the LUMO energy level is estimated to be −2.73 eV. Moreover, the HOMO and LUMO energy levels of the host single strand **4HB-CzNI** were studied in our previous research, and were −5.60 eV and −2.79 eV.[29] According to the electrochemical data, for the hydrogen-bonded

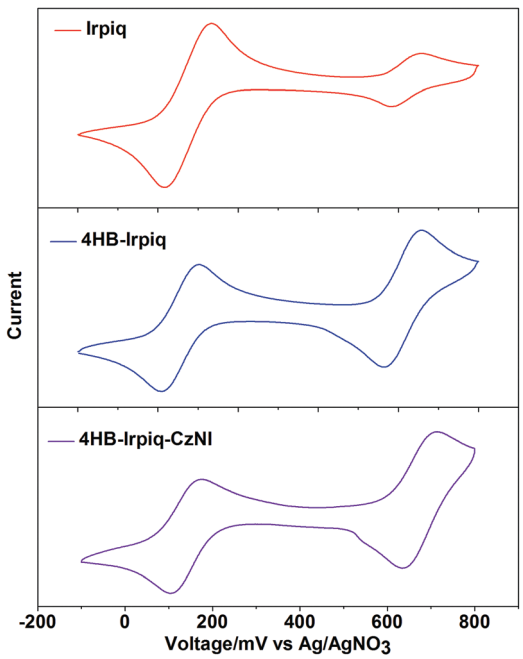

Fig. 7 Cyclic voltammograms of **irpiq**, **4hb-irpiq** and **4hb-irpiq-czni** in 5×10^{-4} mol L^{-1} CH_2Cl_2 solution.

supramolecular **4HB-Irpiq-CzNI**, the HOMO energy level is analogous to that of **4HB-Irpiq**, while the LUMO energy level is analogous to that of **4HB-CzNI**.

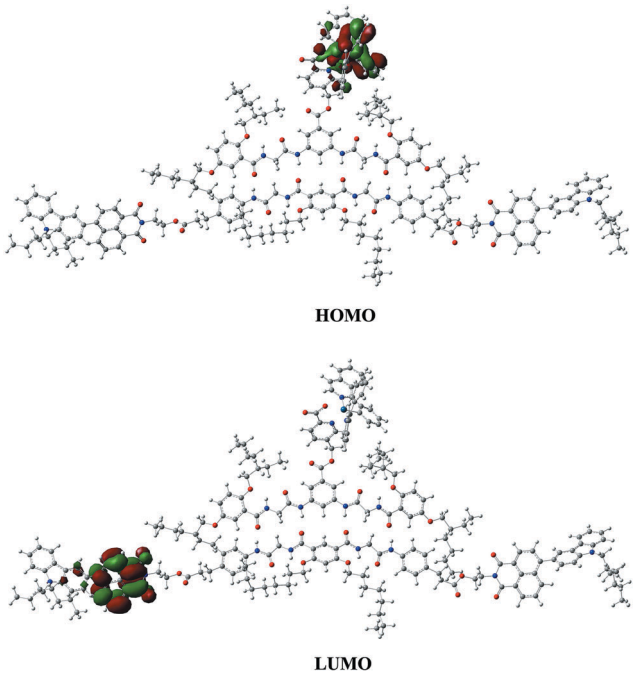

Fig. 8 B3LYP/6-31G*-optimized HOMO and LUMO energy level of the **4hb-irpiq-czni**.

Fig. 8 shows the frontier HOMO and LUMO of the hydrogen-bonded supramolecular **4HB-Irpiq-CzNI**.[42] The HOMO was located on the **Irpiq** in the **4HB-Irpiq** entity, while the LUMO was located on the **CzNI** in the **4HB-CzNI** entity, which were in agreement with the electrochemical results.

Moreover, thermogravimetric analysis (TGA) under nitrogen flow shows that **4HB-Irpiq** and **4HB-Irpiq-CzNI** are thermally stable with 5% weight reduction at temperatures of 254 and 320 °C, respectively (Fig. S2, ESI†). The good thermal stability of target molecule **4HB-Irpiq** and hydrogen-bonded supramolecular **4HB-Irpiq-CzNI** make them promising candidates for OLED applications.

Compared to previous findings, not only is morphological stability at high temperature a key factor determining the performance of OLEDs, but X-ray diffraction (XRD) characterizations of **4HB-Irpiq-CzNI** are also essential for the performance of OLEDs. As shown in Fig. S3a (ESI†), on the one hand, the absence of sharp and intense diffraction signals in both pre- and post-annealed film samples of **4HB-Irpiq-CzNI** suggested its good film amorphism even high temperature. On the other hand, for the small molecular guest compound **Irpiq** newly emerged intense diffraction signals could be discerned in its post-annealed film sample (Fig. S3b, ESI†). What is more, the UV-vis and PL spectra of **4HB-Irpiq-CzNI** were almost the same in both pre- and post-annealed film samples (Fig. S4a and c, ESI†). While, in the region of 300–500 nm, the intensity of the UV-vis spectra of the **Irpiq** differed between pre- and post-annealed film samples (Fig. S4b, ESI†). In addition, the PL spectra of the post-annealed film sample show a slight red-shift from that of the pre-annealed film sample for **Irpiq** (Fig. S4d, ESI†). The differential scanning calorimetry (DSC) curve showed that the small molecular counterpart **Irpiq** exhibited a low phase transition temperature of 72 °C (Fig. S5, ESI†). Therefore, the incorporation of hydrogen-bonded oligoamide strands with **Irpiq** should be beneficial to the enhancement of film amorphism, which is a favorable characteristic for OLEDs.

2.4. Electroluminescent properties

Based on the CV and photophysical experimental results, a two-layered solution-processed OLED using **CzNI** as the host material and **4HB-Irpiq-CzNI** as the emitting guest component was fabricated with a device configuration of ITO/PEDOT:PSS (50 nm)/PVK (50 nm)/**CzNI:4HB-Irpiq-CzNI** (0.11 mol kg^{-1}, 40 wt%) (80 nm)/LiF (0.8 nm)/Al (100 nm) (denoted device **I**), where poly(3,4-ethyl-enedioxythiophene) (PEDOT) acts as the hole-injecting layer, poly(*N*-vinylcarbazole) (PVK) acts as the hole-transporting layer (HTL), and the host–guest blended system acts as the light-emitting layer (EML). To evaluate whether **4HB-Irpiq-CzNI** could act as a promising EL material and to study the structure–property correlation further, a reference device **II** with similar structure to device **I**, but using **Irpiq** as the guest compound was also prepared. For comparison, the host and guest compositions of the emitting layers of devices **I** and **II** are identical (the concentration of **Irpiq** is 0.11 mol kg^{-1}). The relative energy level alignments of the devices are shown in Fig. 9a.

As illustrated in Fig. 9b, the EL spectrum of device **I** is bias-independent. However, a weak emission band at ~520 nm which originated from the emission of the host **CzNI** fluorophore with increasing driving voltage for device **II** (Fig. 9c), implied that incomplete energy transfer occurs between the host and guest compounds during the EL process. Nevertheless, both devices could emit red light with analogous λ_{EL} of ~611 nm. And both devices **I** and **II** show Commission Internationale de l'Éclairage (CIE) coordinates of (0.60, 0.35).

Excitingly, the hydrogen-bonded supramolecular **4HB-Irpiq-CzNI**-based device **I** shows better device performance: with a turn-on voltage (V_{on}) as low as 6.0 V, maximum luminance (L_{max}) as high as 6446 cd m^{-2}, and a maximum current efficiency (LE_{max}) of 7.0 cd A^{-1}, which is among the best performances for all-solution-processed red PhOLEDs. Yet **Irpiq**-based device **II** exhibited a V_{on} of 7.6 V, an L_{max} of 2543 cd m^{-2}, and an LE_{max} of 4.3 cd A^{-1}. According to the current density–voltage–luminance (*J*–*V*–*L*) characteristics of devices **I** and **II** (Fig. 10), the current density of device **I** increases more rapidly than that of device **II** with increasing driving voltage, which accounts for the lower V_{on} of device **I** compared with device **II**. It is noteworthy that device **I** also shows much lower efficiency roll-off than that of device **II** (Fig. 11 and Table 2). For instance, the LE of device **I** remained at 3.9 cd A^{-1} at 1000 cd m^{-2}, while that for device **II** was 1.3 cd A^{-1}; when brightness was at a higher value of 2000 cd m^{-2}, the LE of device **I** was 2.7 cd A^{-1}, but that of device **II** was as low as 0.7 cd A^{-1}. The hydrogen-bonded supramolecular **4HB-Irpiq-CzNI**-based device **I** is high-performance, which may have three main causes: (1) compared with **Irpiq**, there was more effective energy transfer in **4HB-Irpiq-CzNI**. (2) **4HB-Irpiq-CzNI**

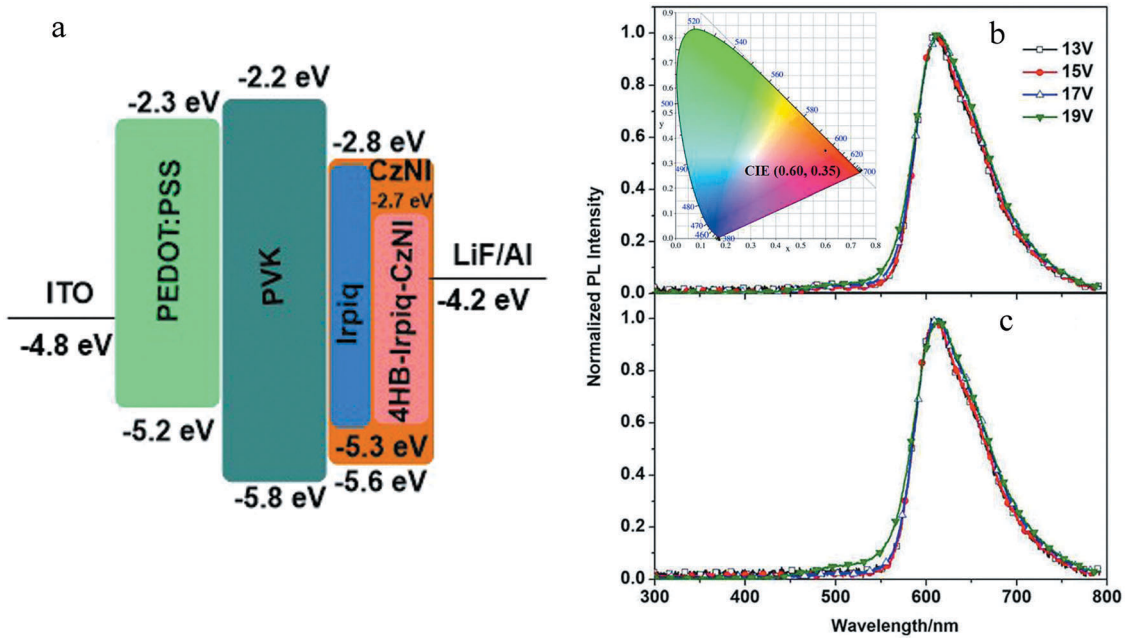

Fig. 9 (a) The relative energy level alignments of devices **i** and **ii**. The EL spectra of devices **i** (b) and **ii** (c).

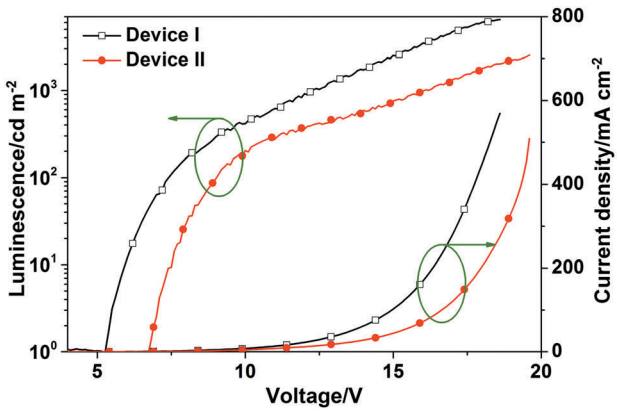

Fig. 10 The current density–voltage–luminance (*j*–*v*–*l*) characteristics of devices **i** and **ii**.

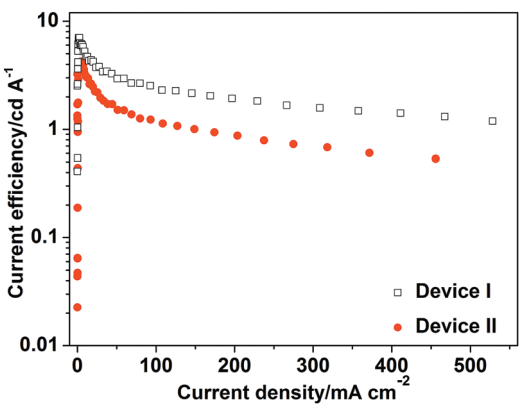

Fig. 11 The luminance efficiency–current density characteristics of devices **i** and **ii**.

Table 2 EL characteristics of devices **I** and **II**

Device	λ_{ELmax} (nm)	V_{on} [a] (V)	L_{max} (cd m^{-2})	LE[b] (cd A^{-1})
I	611	6.0	6446	7.0, 3.9, 3.0, 2.7, 2.2, 1.8, 1.6, 1.3
II	611	7.6	2543	4.3, 1.3, 0.9, 0.7, —, —, —, —

[a] Turn-on voltage recorded at 10 cd m^{-2}. [b] Order of measured value: maximum, then values at 1000, 1500, 2000, 3000, 4000, 5000 and 6000 cd m^{-2} in sequence.

could form stable heteromeric molecular duplexes due to its matched hydrogen-bonding sequences, while the small molecular reference compound **Irpiq** could not form an orderly state. Therefore, the better ordered molecular arrays of **4HB-Irpiq-CzNI** arising from the hydrogen-bonded self-assembly procedures might trigger more efficient carrier transportation within the EML than **Irpiq**.[37] (3) Moreover, the LUMO energy level of **4HB-Irpiq-CzNI** is lower than that of **Irpiq**, which made the injection of electrons easier in device **I**. Furthermore, when the concentration of **4HB-Irpiq-CzNI** increased to 0.17 mol kg^{-1} with a similar device structure to devices **I** and **II**, the performance of this device **III** could be enhanced further with an LE_{max} of 9.1 cd A^{-1} (Fig. S6, ESI†). All these preliminary EL results indicated that the hydrogen-bonded supramolecular **4HB-Irpiq-CzNI** should be suitable as a high-performance electrophosphorescent material.

3. Conclusions

By introducing a small molecule phosphorescent emitter **Irpiq** into an oligoamide strand, hydrogen-bonded single strand **4HB-Irpiq** was synthesized. The guest hydrogen-bonded single strand **4HB-Irpiq** assembled with the host hydrogen-bonded single strand **4HB-CzNI** to obtain a hydrogen-bonded supramolecular

4HB-Irpiq-CzNI *via* H-bond interactions. Compared with the small molecular counterparts **CzNI** and **Irpiq**, the hydrogen-bonded supramolecular **4HB-Irpiq-CzNI** not only exhibits better energy transfer efficiency according to photophysical research, but also a dramatically enhanced EL performance, maximum luminance as high as 6446 cd m^{-2}, and maximum current efficiency of 7.0 cd A^{-1}, which is among the best performances for all-solution-processed red PhOLEDs. When the concentration of **4HB-Irpiq-CzNI** was increased, the maximum current efficiency could reach 9.1 cd A^{-1}, which is the best current efficiency for all-solution-processed red PhOLEDs so far. Our research findings demonstrated that the introduction of an oligoamide motif into a phosphorescent emitter is an effective way to develop high-performance PhOLEDs.

4. Experimental section

General information and methods

All the commercially available chemicals were used directly without further purification unless otherwise stated. All the solvents were of analytical grade and freshly distilled prior to use. Anhydrous *N*,*N*-dimethylformamide and dichloromethane were refluxed with calcium hydride respectively, followed by fresh distillation before use. 1D ^{1}H NMR, ^{13}C NMR and 2D ^{1}H NMR (NOESY) spectra were recorded on Bruker AVANCE-400 and Bruker AVANCE-600 spectrometers in $CDCl_3$ using TMS as the internal standard. High resolution MS spectra were measured with a Q-TOF Premier ESI mass spectrometer (Micromass, Manchester, UK). Thermogravimetric analysis (TGA) was performed on a Discovery TGA instrument under nitrogen atmosphere at a heating rate of 1 °C min^{-1}. Differential scanning calorimetry (DSC) was performed under a flow of nitrogen at a heating rate of 10 °C min^{-1} with NETZSCH DSC-214-Polyma. UV-Vis absorption spectra of the 10^{-5} mol L^{-1} CH_2Cl_2 solution and solid thin film samples were measured on a PerkinElmer Lambda 950 scanning spectrophotometer. PL spectra of both the dilute solution (10^{-5} mol L^{-1} in CH_2Cl_2) and thin-film samples were recorded on an LS-55 fluorescence spectrophotometer at 298 K. The absolute PL quantum yields of the compounds in the thin solid states were determined on a HORIBA Jobin Yvon Fluoromax-4 spectrophotometer with an integrating sphere under ambient conditions. The decay curves of the devices were detected using a HORIBA TEMPRO-01 transient spectrometer. Samples for atomic force microscopy (AFM) measurements were prepared by spin-casting from **Irpiq** and **4HB-Irpiq** in chloroform solution on glass substrates with HERZAN-T5-150. Cyclic voltammetry (CV) measurements were carried out on a CHI830B electrochemical workstation at room temperature in anhydrous dichloromethane solution with 0.1 mol L^{-1} tetrabutylammonium perchlorate as the supporting electrolyte at a scanning rate of 100 mV s^{-1}. The CV system was constructed using a platinum plate, an $Ag/AgNO_3$ (0.1 mol L^{-1} in acetonitrile) electrode and a platinum wire as the working electrode, quasi-reference electrode and counter electrode, respectively. Each measurement was calibrated with a ferrocene/ferrocenium (Fc/Fc^+) redox couple as the internal standard. The OLEDs structure employed in this study is: ITO/PEDOT:PSS (3000 rpm)/PVK (1500 rpm)/emitter (80 nm)/LiF (0.8 nm)/Al (100 nm), where PEDOT poly(3,4-ethylenedioxythiophene) acts as the anode buffer material and PVK [poly(*N*-vinylcarbazole)] acts as the hole transporting material. Prior to use, the indium–tin oxide (ITO) (with a sheet resistance of 20 Ω $\square^{-1}$ and a thickness of 120 nm) precoated glass substrate was cleaned in ultrasonic baths of detergent solution, deionized water, acetone, and 2-propanol in sequence. After degreasing, the ITO substrate was oxidized and cleaned in a UV–ozone chamber under oxygen plasma for 15 min. Thin films of PVK and emissive layers were prepared from solutions with concentrations of 6 mg mL^{-1} chlorobenzene and *p*-xylene, respectively, by spin-coating at 1500 rpm in a glove box (VAC Co.) with N_2 circulation (with <1 ppm oxygen and water). The deposition of an electron-injecting LiF (0.8 nm) layer followed by an Al capping layer (100 nm) was realized through a shadow mask in a vacuum chamber of $\sim 3 \times 10^{-4}$ Pa, and the layer thickness was monitored by a crystal thickness monitor (Sycon). The current density–voltage–luminance characteristics of the OLEDs were recorded on a calibrated silicon photodiode driven by KEITHLEY-2400.

Synthesis of 3. Compound **1** (500.0 mg, 0.4 mmol), 5-(hydroxymethyl) picolinic acid **2** (132.2 mg, 0.9 mmol), Na_2CO_3 (410.0 mg, 10 mmol), and 60 mL of 1,2-dichloroethane were added into a 100 mL two-necked flask. And then the system was stirred under Ar atmosphere at 83.5 °C for 15 h. After **1** was consumed completely according to TLC analysis, the system was cooled to room temperature. Then it was extracted with CH_2Cl_2, washed with brine, and then dried over anhydrous sodium sulfate. Removal of the solvent under vacuum resulted in the crude product, which was purified by column chromatography (silica gel, CH_2Cl_2 : MeOH = 20 : 1, v/v) to afford compound **3** as a red solid with yield of 70%. M.p.: 284–285 °C. ^{1}H NMR (400 MHz, DMSO-d_6) δ (ppm): 9.02 (t, J = 8.0 Hz, 2H, ArH), 8.49 (d, J = 6.4 Hz, 1H, ArH), 8.35 (d, J = 8.0 Hz, 1H, ArH), 8.27 (d, J = 8.0 Hz, 1H, ArH), 8.12–8.07 (m, 3H, ArH), 7.05 (d, J = 8.0 Hz, 1H, ArH), 7.89–7.84 (m, 5H, ArH), 7.67 (d, J = 6.4 Hz, 1H, ArH), 7.53 (s, 1H, ArH), 7.48 (d, J = 6.0 Hz, 1H, ArH), 7.03 (t, J = 7.2 Hz, 1H, ArH), 6.97 (t, J = 7.2 Hz, 1H, ArH), 6.80 (t, J = 7.2 Hz, 1H, ArH), 6.71 (t, J = 7.2 Hz, 1H, ArH), 6.38 (d, J = 7.2 Hz, 1H, ArH), 6.06 (t, J = 7.2 Hz, 1H, ArH), 4.37 (t, J = 5.2 Hz, 2H, $-CH_2$).

Synthesis of 4HB-Irpiq. **4** (493.7 mg, 0.5 mmol) and DMAP (4-dimethylaminopyridine) (122.2 mg, 1.0 mmol) were dissolved in 30 mL of CH_2Cl_2 under Ar atmosphere at 0 °C. The solution was stirred at 0 °C for 1 hour, then **3** (150 mg, 0.2 mmol) and EDCI (-ethyl-3-(3-dimethylaminopropyl)carbodiimide hydrochloride) (191.7 mg, 1.0 mmol) was added. The reaction mixture was stirred for 48 hours at room temperature. The mixture was directly subjected to silica gel column chromatography to afford the desired product **4HB-Irpiq** as a red solid in 13% yield; m.p.: 97–98 °C. ^{1}H NMR (400 MHz, $CDCl_3$, δ): 8.96 (s, 2H, –NH), 8.91–8.87 (m, 1H, ArH), 8.80–8.75 (m, 3H, NH, ArH), 8.72 (d, J = 6.4 Hz, 1H, ArH), 8.37 (d, J = 7.6 Hz, 1H, ArH), 8.19 (d, J = 8.0 Hz, 1H, ArH), 7.98 (d, J = 8.4 Hz, 2H, ArH), 7.91–7.88 (m, 1H, ArH),

7.76–7.73 (m, 5H, ArH), 7.70–7.68 (m, 2H, ArH), 7.65–7.63 (m, 2H, ArH), 7.55 (d, J = 6.4 Hz, 1H, ArH), 7.47 (s, 1H, ArH), 7.31 (d, J = 7.0 Hz, 1H, ArH), 7.11 (d, J = 5.2 Hz, 1H, ArH), 7.02 (dd, J = 9.2 Hz, J = 3.2 Hz, 2H, ArH), 6.97–6.86 (m, 4H, ArH), 6.73 (t, J = 7.6 Hz, 1H, ArH), 6.65 (t, J = 7.6 Hz, 1H, ArH), 6.42 (d, J = 7.6 Hz, 1H, ArH), 6.15 (d, J = 7.2 Hz, 1H, ArH), 4.21 (s, 4H; CH_2), 3.99 (s, 4H; CH_2), 3.85 (d, J = 5.6 Hz, 4H, CH_2), 1.85–1.79 (m, 2H, CH_2), 1.72–1.69 (m, 2H; CH_2), 1.52–1.29 (m, 28H; CH_2), 0.93–0.82 (m, 28H; CH_2; CH_3). ^{13}C NMR (100 MHz, DMSO-d_6, δ): 172.5, 170.0, 168.3, 167.6, 166.5, 153.5, 151.6, 145.9, 145.6, 140.7, 138.6, 136.7, 132.9, 131.0, 130.3, 129.6, 128.2, 127.7, 126.9, 126.5, 126.2, 121.5, 121.1, 120.8, 120.4, 116.4, 113.8, 72.3, 71.2, 62.9, 45.5, 39.4, 39.2, 30.7, 30.5, 29.7, 29.1, 29.0, 24.1, 23.8, 23.1, 23.0, 14.1, 11.1, 11.0. HRMS (ESI) m/z: $[M + Na]^+$ calcd for $C_{94}H_{110}IrN_7O_{12}Na$, 1744.7734; found, 1744.7743.

Conflicts of interest

There are no conflicts to declare.

Acknowledgements

We acknowledge the financial support for this work by the National Natural Science Foundation of China (No. 21372168 and 11474018). We also thank the Analytical & Testing Center, Sichuan University and Comprehensive Training Platform of Specialized Laboratory, College of Chemistry, Sichuan University for providing NMR and HRMS data for the intermediates and target molecules and Interdisciplinary Research Center on Biology and Chemistry, Shanghai Institute of Organic Chemistry, Chinese Academy of Sciences for providing the calculation of the structure of the target molecule.

References

1 P. C. Xue, J. P. Ding, P. P. Wang and R. Lu, *J. Mater. Chem. C*, 2016, **4**, 6688.
2 X. L. Yang, G. J. Zhou and W. Y. Wong, *Chem. Soc. Rev.*, 2015, **44**, 8484.
3 S. Schmidbauer, A. Hohenleutner and B. Konig, *Adv. Mater.*, 2013, **25**, 2114.
4 L. M. Xie, J. Y. Zhuang, X. L. Chen, Z. Z. Xie, R. F. He, L. Chen, W. L. Wang, D. Y. Zhang, W. M. Su, J. X. Tang, X. L. Yan and Z. Cui, *ACS Photonics*, 2017, **4**, 449.
5 Y. Wang, Y. M. Lu, B. X. Gao, S. M. Wang, J. Q. Ding, L. X. Wang, X. B. Jing and F. S. Wang, *Chem. Commun.*, 2016, **52**, 11508.
6 X. L. Wang, Y. Ma, S. Y. Feng, L. Wang, J. F. Li and J. L. Zhang, *Org. Electron.*, 2017, **41**, 251.
7 Y. M. Zhang, F. Y. Meng, C. F. You, S. Y. Yang, L. Xiong, W. J. Xiong, W. G. Zhu, Y. F. Wang, Y. Pei and S. J. Su, *Dyes Pigm.*, 2017, **142**, 457.
8 Y. F. Chang, Y. C. Chiu, H. W. Chang, Y. S. Wang, Y. L. Shih, C. H. Wu, Y. L. Liu, Y. S. Lin, H. F. Meng, Y. Chi, H. L. Huang, M. R. Tseng, H. W. Lin, H. W. Zan, S. F. Horng and J. Y. Juang, *J. Appl. Phys.*, 2013, **114**, 123101.
9 K. Y. Zhang, X. J. Chen, G. L. Sun, T. W. Zhang, S. J. Liu, Q. Zhao and W. Huang, *Adv. Mater.*, 2016, **28**, 7137.
10 X. F. Wei, W. Y. Tan, J. H. Zou, Q. X. Guo, D. Y. Gao, D. G. Ma, J. B. Peng, Y. Cao and X. H. Zhu, *J. Mater. Chem. C*, 2017, **5**, 2329.
11 Y. Ma, J. Yang, S. J. Liu, H. T. Xia, P. F. She, R. Jiang and Q. Zhao, *Adv. Opt. Mater.*, 2017, 1700587.
12 J. M. Han, S. Guo, J. Wang, L. W. Wei, Y. L. Zhuang, S. J. Liu, Q. Zhao, X. W. Zhang and W. Huang, *Adv. Opt. Mater.*, 2017, 1700359.
13 D. X. Ma, Y. Qiu and L. Duan, *Adv. Funct. Mater.*, 2016, **26**, 3438.
14 S. Guo, T. C. Huang, S. J. Liu, K. Y. Zhang, H. R. Yang, J. M. Han, Q. Zhao and W. Huang, *Chem. Sci.*, 2017, **8**, 348.
15 S. Z. Cao, L. Hao, W. Y. Lai, H. Zhang, Z. Yu, X. W. Zhang, X. Liu and W. Huang, *J. Mater. Chem. C*, 2016, **4**, 4709.
16 X. J. Liu, B. Yao, Z. L. Zhang, X. F. Zhao., B. H. Zhang, W. Y. Wong, Y. X. Cheng and Z. Y. Xie, *J. Mater. Chem. C*, 2016, **4**, 5787.
17 S. F. Xue, Y. J. Wu, Y. S. Lu, X. Xu, Q. K. Sun and W. J. Yang, *J. Mater. Chem. C*, 2017, **5**, 11700.
18 P. Tao, Y. B. Zhang, J. Wang, L. W. Wei, H. X. Li, X. L. Li, Q. Zhao, X. W. Zhang, S. J. Liu, H. Wang and W. Huang, *J. Mater. Chem. C*, 2017, **5**, 9306.
19 Y. M. Han, L. B. Bai, C. R. Yin, C. J. Ou, X. W. Zhang, Z. Y. Zuo, B. Liu, M. N. Yu, J. Y. Lin, J. F. Zhao, W. S. Zhu, Y. Y. Liu, J. W. Li, J. P. Wang, L. H. Xie and W. Huang, *J. Mater. Chem. C*, 2017, **5**, 9903.
20 W. Cho, G. Sarada, A. Maheshwaran, Y. S. Gal, Y. Nam, J. Y. Lee and S. H. Jin, *J. Mater. Chem. C*, 2017, **5**, 10029.
21 X. Q. Liao, X. Yang, R. Zhang, J. Cheng, J. Li, S. Y. Chen, J. Zhu and L. Li, *J. Mater. Chem. C*, 2017, **5**, 10001.
22 T. M. Zhang, J. Sun, X. Q. Liao, M. N. Hou, W. H. Chen, J. Li, H. Wang and L. Li, *Dyes Pigm.*, 2017, **139**, 611.
23 J. Zhao, M. Lian, Y. Yu, X. G. Yan, X. B. Xu, X. L. Yang, G. J. Zhou and Z. X. Wu, *Macromol. Rapid Commun.*, 2015, **36**, 71.
24 F. Xu, H. U. Kim, J. H. Kim, B. J. Jung, A. C. Grimsdale and D. H. Hwang, *Prog. Polym. Sci.*, 2015, **47**, 92.
25 D. Konkolewicz, A. Grayweale and S. Perrier, *J. Am. Chem. Soc.*, 2009, **131**, 18075.
26 C. W. Wu and H. C. Lin, *Macromolecules*, 2006, **39**, 7985.
27 M. Trollsås and J. L. Hedrick, *J. Am. Chem. Soc.*, 1998, **120**, 4644.
28 S. H. M. Söntjens, R. P. Sijbesma, M. H. P. V. Genderen and E. W. Meijer, *J. Am. Chem. Soc.*, 2000, **122**, 7487.
29 C. Zhang, Y. Wang, Q. Y. Huang, J. Zhou, Y. Huang, S. L. Zhao and Z. Y. Lu, *Dyes Pigm.*, 2018, **149**, 755.
30 Y. Wang, J. Zhou, X. Wang, X. J. Zheng, Z. Y. Lu, W. Zhang, Y. Q. Chen, Y. Huang, X. M. Pu and J. S. Yu, *Dyes Pigm.*, 2014, **100**, 87.
31 S. J. Yang, J. S. You, J. B. Lan and G. Gao, *J. Am. Chem. Soc.*, 2012, **134**, 11868.
32 B. Liang, C. Y. Jiang, Z. Chen, X. J. Zhang, H. H. Shi and Y. Cao, *J. Mater. Chem.*, 2006, **16**, 1281.
33 B. Gong, Y. F. Yan, H. Q. Zeng, E. S. Jankunn, Y. W. Kim, J. Zhu and H. Ickes, *J. Am. Chem. Soc.*, 1999, **121**, 5607.

34 H. Q. Zeng, R. S. Miller, R. A. Flowers and B. Gong, *J. Am. Chem. Soc.*, 2000, **122**, 2635.
35 H. Q. Zeng, X. W. Yang, A. L. Brown, S. Martinovic, R. D. Smith and B. Gong, *Chem. Commun.*, 2003, 1556.
36 M. F. Li, K. Yamato, J. S. Ferguson and B. Gong, *J. Am. Chem. Soc.*, 2006, **128**, 12628.
37 J. J. Liu, Y. Wang, G. D. Lei, J. B. Peng, Y. Huang, Y. Cao, M. G. Xie, X. M. Pu and Z. Y. Lu, *J. Mater. Chem.*, 2009, **19**, 7753.
38 J. J. Liu, Y. H. Li, Y. Wang, H. Q. Sun, Z. Y. Lu, H. B. Wu, J. B. Peng and Y. Huang, *Opt. Mater.*, 2012, **34**, 1535.
39 P. K. Poddutoori, L. P. Bregles, G. N. Lim, P. Boland, R. G. Kerr and F. D'Souza, *Inorg. Chem.*, 2015, **54**, 8482.
40 V. Bandi, F. P. D'Souza, H. B. Gobeze and F. D'Souza, *Chemistry*, 2015, **21**, 2669.
41 M. Suresh, A. K. Mandal, E. Suresh and A. Das, *Chem. Sci.*, 2013, **4**, 2380.
42 M. J. Frisch, G. W. Trucks, H. B. Schlegel, G. E. Scuseria, M. A. Robb, J. R. Cheeseman, G. Scalmani, V. Barone, B. Mennucci, G. A. Petersson, H. Nakatsuji, M. Caricato, X. Li, H. P. Hratchian, A. F. Izmaylov, J. Bloino, G. Zheng, J. L. Sonnenberg, M. Hada, M. Ehara, K. Toyota, R. Fukuda, J. Hasegawa, M. Ishida, T. Nakajima, Y. Honda, O. Kitao, H. Nakai, T. Vreven, J. A. Montgomery, Jr., J. E. Peralta, F. Ogliaro, M. Bearpark, J. J. Heyd, E. Brothers, K. N. Kudin, V. N. Staroverov, R. Kobayashi, J. Normand, K. Raghavachari, A. Rendell, J. C. Burant, S. S. Iyengar, J. Tomasi, M. Cossi, N. Rega, J. M. Millam, M. Klene, J. E. Knox, J. B. Cross, V. Bakken, C. Adamo, J. Jaramillo, R. Gomperts, R. E. Stratmann, O. Yazyev, A. J. Austin, R. Cammi, C. Pomelli, J. W. Ochterski, R. L. Martin, K. Morokuma, V. G. Zakrzewski, G. A. Voth, P. Salvador, J. J. Dannenberg, S. Dapprich, A. D. Daniels, O. Farkas, J. B. Foresman, J. V. Ortiz, J. Cioslowski and D. J. Fox, *Gaussian 09, Revision A.01*, Gaussian, Inc., Wallingford CT, 2009.